



Direct Measurements of Ozone Response to Emissions Perturbations in California

Shenglun Wu¹, Hyung Joo Lee², Andrea Rohrbacher³, Shang Liu², Toshihiro Kuwayama², John H. Seinfeld⁴, and Michael J. Kleeman¹

5 ¹Department of Civil and Environmental Engineering, University of California Davis, 1 Shields Ave, Davis, CA 95616, USA

²Department of Chemistry, University of California Irvine, Irvine, CA 92697, USA

³Research Division, California Air Resources Board, 1001 I Street, Sacramento, CA 95814, USA

10 ⁴Department of Chemical Engineering, California Institute of Technology, 1200 E. California Blvd, Pasadena, CA 91125, USA

Correspondence to: Michael J. Kleeman (mjkleeman@ucdavis.edu)

Abstract.

15 A new technique was used to directly measure O₃ response to changes in precursor NO_x and VOC concentrations in the atmosphere using three identical Teflon “smog chambers” equipped with UV lights. One chamber served as the baseline measurement for O₃ formation, one chamber added NO_x, and one chamber added surrogate VOCs (ethylene, m-xylene, n-hexane). Comparing the O₃ formation between chambers over a three-hour UV cycle provides a direct measurement of O₃ sensitivity to precursor concentrations. Measurements made with this system at Sacramento, California, between April 2020 – December 2020 revealed that the atmospheric chemical regime followed a seasonal cycle. O₃ formation was VOC-limited (NO_x – rich) during the early spring, transitioned to NO_x-limited during the summer due to increased concentrations of ambient VOCs with high O₃ formation potential, and then returned to VOC-limited (NO_x-rich) during the fall season as the concentrations of ambient VOCs decreased and NO_x increased. This seasonal pattern of O₃ sensitivity is consistent with the cycle of biogenic emissions in California. The direct chamber O₃ sensitivity measurements matched semi-direct measurements of HCHO/NO₂ ratios from the
25 TROPOspheric Monitoring Instrument (TROPOMI) onboard the Sentinel-5 Precursor (Sentinel-5P) satellite. Furthermore, the satellite observations showed that the same seasonal cycle in O₃ sensitivity occurred over most of the entire state of California, with only the urban cores of the very large cities remaining VOC-limited across all seasons. Looking at the entire measurement period, days with baseline chamber O₃ concentrations above 90 ppb had median O₃ sensitivity that was NO_x-limited, suggesting that a NO_x emissions control strategy would be most effective at reducing these peak O₃ concentrations. In contrast, days with O₃ concentrations below 80 ppb had median O₃ sensitivity that was VOC-limited, suggesting that an emissions control strategy focusing on NO_x reduction would increase O₃ concentrations. VOC controls on these intermediate days would be difficult, however, if biogenic VOCs account for the majority of the O₃ formation. This challenging situation suggests that emissions control programs that focus on NO_x reductions will immediately lower peak O₃ concentrations, but slightly increase intermediate O₃
35 concentrations until NO_x levels fall far enough to re-enter the NO_x-limited regime. The spatial pattern of increasing and decreasing O₃ concentrations in response to a NO_x emissions control strategy should be carefully mapped in order to fully understand the public health implications.



1 Introduction

Ground-level ozone (O_3) is an oxidant that inflames airways and damages tissue in the respiratory tract leading to increased coughing, wheezing, shortness of breath, and other asthmatic symptoms (US EPA, 2020b). Daily maximum 8-hour average O_3 concentrations designed to protect public health are codified in the National Ambient Air Quality Standards (NAAQS) (US EPA, 2021) and the California Ambient Air Quality Standards (CAAQS) (California Air Resources Board, 2007). Seven of the ten cities across the United States with the highest O_3 concentrations are located in California (American Lung Association, 2020), making O_3 pollution a continued public health threat for millions of California residents more than four decades after O_3 abatement efforts began.

O_3 levels are often described by the maximum 8-hr average concentration that occurs within each day. The annual fourth-highest daily maximum 8-hr average concentration averaged over three years has special regulatory significance. This “design value” determines whether the region containing the monitor complies with the NAAQS. O_3 design values in California decreased steadily between the years 1980 and 2019 (Figure 1) due to the success of emissions control programs that reduced concentrations of precursors broadly divided into two groups: oxides of nitrogen (NO_x) and volatile organic compounds (VOCs) (Parrish et al., 2016; Simon et al., 2015). Continued progress after the year 2010 has been slower, and O_3 design values even increased in some air basins between the years 2015 – 2018 (Figure 1). Multiple factors have been proposed to explain these increasing O_3 concentrations including (i) growing importance of precursor VOC emissions not previously accounted for in the planning process as major sources such as transportation have been controlled (McDonald et al., 2018; Shah et al., 2020), (ii) an imbalance in the historical degree of NO_x and VOC reductions (Cox et al., 2013; Steiner et al., 2006), or (iii) the consequences of climate change (Jacob and Winner, 2009; Jing et al., 2017; Pusede et al., 2015; Rasmussen et al., 2013; Weaver et al., 2009). All these theories are supported to varying degrees by indirect measurements or model predictions, but there is an absence of strong direct evidence that identifies dominant factors contributing to the increased O_3 concentrations. The uncertainty that lingers over the recent O_3 trends suggests that fresh approaches are needed to directly verify the optimum emissions control path.

O_3 formation has been studied for decades in California, using both measurements and model simulations (Kroll et al., 2020). These past studies provide important background information about the effects of precursor NO_x and VOC species and help build the foundation for new studies. Statistical analyses of long-term surface measurements have determined that lower NO_x concentrations are associated with higher O_3 concentrations on weekends (Pollack et al., 2012; Pusede and Cohen, 2012) and higher temperatures are associated with increased VOC emissions and chemical reaction rates, leading to higher O_3 concentrations during warm stagnation events (Lafranchi et al., 2011; Nussbaumer and Cohen, 2020). These long-term studies suggest that VOCs are the limiting precursor for O_3 formation in the center of large cities, while NO_x is the limiting precursor in downwind areas (Lafranchi et al., 2011; Pusede and Cohen, 2012). Neither long-term analysis method clearly explains the recent trend of increasing O_3 concentrations in Los Angeles.



75 O₃ sensitivity has also been analyzed over shorter timescales using ratios of photochemical “indicator” species
including H₂O₂/HNO₃ and HCHO/NO₂ (Sillman, 1995; Tonnesen and Dennis, 2000). Satellite retrievals of
HCHO/NO₂ from Global Ozone Monitoring Experiment (GOME), SCanning Imaging Absorption spectroMeter for
Atmospheric CartographY (SCIAMACHY), and Ozone Monitoring Instrument (OMI) have extended these O₃
80 sensitivity calculations over broad geographical regions with 13 km × 24 km resolution (Duncan et al., 2010; Jin et
al., 2017; Martin et al., 2004; Schroeder et al., 2017). The short-term measurements generally support the findings
from the long-term studies but once again fail to identify the dominant factor(s) driving the recent increase in O₃
design values. Reactive chemical transport models (CTMs) have been used extensively to predict the effectiveness
of candidate emissions control programs (Brown, 2018; California Air Resources Board, 2018; Meng et al., 1997;
Sillman, 1999) and so one might expect that they would provide the most detailed explanation for recent O₃ trends.
85 Models are necessarily incomplete approximations to highly complex real-world systems, and so they are often
incapable of predicting subtle features in pollutant trends. No model calculation has been able to reproduce the
observed increase in O₃ design values (Parrish et al., 2017). It is unclear whether this failure stems from a lack of
accurate emissions trends, an incomplete description of atmospheric chemistry, or an incomplete representation of the
effects of shifting climate on O₃ formation mechanisms.

90

Recent advances in measurement techniques provide new tools to study O₃ sensitivity directly. Transportable smog
chambers have been demonstrated to measure O₃ formation potential in the real atmosphere (Howard et al., 2008,
2010) and to bridge the gap between laboratory studies of photochemical reactions leading to secondary pollutants
formation and the real atmosphere (Jorga et al., 2020). At the same time, the satellite TROPOspheric Monitoring
95 Instrument (TROPOMI) launched by the European Space Agency (ESA) in October 2017 provides measurements of
HCHO and NO₂ tropospheric vertical column densities (TVCDs) with 3.5 km × 5.5 km spatial resolution that can start
to resolve O₃ perturbations around major sources such as wildfires (Ialongo et al., 2020; Veefkind et al., 2012;
Vigouroux et al., 2020). The purpose of this study is to combine these two new measurement techniques into a detailed
analysis of O₃ sensitivity to precursor NO_x and VOC emissions spanning an entire spring-summer-fall cycle in
100 California. Daily measurements from smog-chamber perturbation experiments are analysed for short-term trends
(day-of-week) and long-term trends (seasonal variation) to reveal the effects of traffic, natural vegetation, and
wildfires. The direct O₃ sensitivity measurements are then combined with TROPOMI HCHO/NO₂ ratios to extend
our understanding of the O₃ sensitivity across the entire state of California.

2. Methods

105 2.1 Ground-based measurement

Three identical transportable smog chambers were used to directly measure basecase O₃ concentration and O₃
sensitivity to precursor NO_x and VOC. Each chamber was constructed from fluorinated ethylene propylene (FEP)
with a volume of 1 m³ housed in an enclosure measuring 2.13 m H x 1.22 m L x 1.22 m W. UV lamp panels were
placed on the floor and the roof of the chamber support frame. Each panel can hold up to six UV lamps (Sylvania,



110 F40BL 40W T12) that emit at wavelengths between 280–400 nm. The lamp panels were configured to produce 50
W/m² to replicate the mid-day photochemistry in California during the summer. The enclosure walls were constructed
from polished aluminium with total reflectivity of ~95%. Figure S1 represents the cross-sectional view of the
transportable smog chamber system.

115 One cubic meter of ambient air was injected into the FEP chambers at the start of an experiment using a Teflon
diaphragm pump (Model DOA-V751-FB, Gas Manufacturing, Benton Harbor, MI, USA) operating at a flow rate of
10 L·min⁻¹ for each chamber. Solenoid valves were configured to inject perturbation gases NO_x (8 ppb NO₂) and
VOC surrogates (4.4 ppb ethylene, 2.8 ppb n-hexane, and 0.8 ppb m-xylene) respectively into chambers #1 and #3 for
120 comparison to basecase chamber #2. Perturbation gases were added halfway through the chamber filling operation so
that they would be thoroughly mixed with the ambient air during the remainder of the chamber filling process. The
composition of the VOC perturbation was based on the VOC mixture used to determine ozone formation potential
(Carter et al., 1995). The magnitude of the perturbations was selected to be as small as possible while still generating
an observable change in monitored ozone concentrations. A single set of monitors sequentially measured
125 concentrations within each chamber to increase the precision of the inter-chamber comparisons. The current
experiment includes measurements of NO_x (Model nCLD-855-Yh, ECO Physics, Duernten, Switzerland), NO_y (sum
of all oxidized atmospheric odd-nitrogen species) (Model 42i, Thermo Fisher, Franklin, MA, USA), O₃ (Model 205,
2B technology, Boulder, CO, USA), and temperature – relative humidity sensor (Model RH-USB, Omega
Engineering, Norwalk, CT, USA). Chambers were drained at the conclusion of an experiment using a rotary vane
vacuum pump (Model 0523-101Q-G588DX, Gast Manufacturing, Benton Harbor, MI, USA). All chamber operations
130 were controlled automatically using a program written in LabView that interfaced with a customized set of data
acquisition devices and solenoid valves (DAQ-SV).

The consistency of the O₃ formation rates across chambers was tested in a controlled laboratory environment prior to
deployment in the field. All three 1 m³ FEP chambers were filled with laboratory air and were perturbed by an equal
135 mixture of both NO_x and VOC prior to 180 min of UV exposure. A t-test applied to the final concentrations suggests
that the final O₃ concentrations in all three chambers were identical with a confidence level of 88–90%. Figure S2
illustrates the agreement between chamber #1 and #3 O₃ measurements vs. chamber #2 O₃ measurements during a
typical QA/QC check. The loss rate of O₃ to chamber walls was determined in the dark for all three 1 m³ FEP chambers
filled with identical NO_x-VOC mixtures. Average loss rates of 5% hr⁻¹ were calculated over the 3-hour experiments.
140 Loss rates were identical for all chambers in the system and so this issue will not influence the comparisons between
chambers in the current study.

O₃ formation in the basecase chamber was compared to ambient O₃ measurements at a nearby monitoring station to
confirm that the chamber accurately represents the behaviour observed in the atmosphere. Results from a preliminary
145 test conducted at three locations around Los Angeles, California, are shown in Figure S3. The initial O₃ concentration
in the basecase chamber was similar to the ambient O₃ concentration, indicating that the gas-phase chemical



composition related to O₃ formation is not modified during chamber injection. The initial rate of O₃ formation in the basecase chamber using UV lights was also similar to the rate of O₃ formation in the atmosphere. O₃ formation in the basecase chamber is approximately constant for the entire duration of the experiment on each day, but the ambient O₃ formation rates typically decrease in the early afternoon as the atmospheric mixing dilutes the polluted surface layer with clean air from above. The O₃ formation in the chamber, therefore, captures a realistic “worst-case scenario” for surface-level O₃ formation under conditions where atmospheric mixing cannot dilute the NO_x and VOC concentrations that build up in the nocturnal ground-level stagnation layer.

VOC measurements are useful to help interpret O₃ formation trends and to identify the chemical regime on the NO_x-VOC isopleth for O₃ (Seinfeld and Spyros N. Pandis., 2016). Ground-level daily VOC measurements from Photochemical Assessment Monitoring Stations (PAMS) are only available for a limited number of summer months and so alternative indicator species were investigated. Baker (2008) found that non-methane hydrocarbon (NMHC) concentrations were correlated with CO concentrations in 28 U.S. cities during the years 1999 – 2005. This may reflect situations where dominant sources that emit CO also emit large amounts of NMHC, or it may reflect situations where relatively constant sources of CO and NMHC are correlated because they are diluted by the same amount of atmospheric mixing. The success of emissions control programs targeting anthropogenic VOCs has increased the relative importance of residual biogenic VOCs in many urban atmospheres across the US (US EPA, 2020a). Biogenic sources do not emit CO and so any correlation between biogenic VOCs and CO purely reflects the utility of CO as an indicator of atmospheric mixing that equally affects all sources. In an effort to improve the ability of CO to represent biogenic VOCs in the current study, an additional metric was calculated by multiplying the measured CO concentrations by the temperature and relative humidity-induced enhancement factor for isoprene emissions (Guenther et al., 1991). Figure S4 shows the correlation between measured VOC reactivity (VOCR) and CO*Biogenic at Sacramento during summer months between 2010 – 2019. VOCR was calculated from PAMS measurements of VOC concentrations multiplied by their reaction rate constant with OH (Chen et al., 2010; Kleinman, 2005; Steiner et al., 2008). VOCR and CO*Biogenic are reasonably well correlated ($r = 0.6$, $p < 0.001$), while VOCR and CO were less correlated ($r = 0.39$). This analysis supports the preference for CO*Biogenic as an approximate surrogate for VOCR in the current study.

2.2 Satellite data

Tropospheric HCHO and NO₂ retrievals (Level 2; Unit: mol/m²) over California were obtained from the TROPOMI for February – October 2020. The TROPOMI is onboard the Sentinel-5 Precursor (Sentinel 5-P) satellite, which was launched by the ESA in October 2017. The polar-orbiting satellite enables quantitative information on trace gases to be retrieved approximately at 13:30 local sun time (ascending node) each day on a global scale. The spatial resolution of TROPOMI NO₂ and HCHO TVCDs are 3.5 km × 5.5 km, which is finer than that of the predecessor OMI (13 km × 24 km). Quality assurance (QA) values were obtained alongside the HCHO and NO₂ data, and only measurements with QA values ≥ 0.50 were retained for further analyses. Daily TROPOMI measurements were used to calculate



monthly averages to reduce errors in daily TROPOMI data. Further details about the TROPOMI data are provided by Veefkind et al. (2012), Van Geffen et al.(2020), and De Smedt et al.(2018).

2.3 Experimental description

185 O₃ sensitivities to precursor NO_x/VOC concentrations were measured in central Sacramento, CA (N 38.57, W 121.49)
from April – December 2020. Sources in the vicinity of the site include commercial office buildings, restaurants, two
major highways, freight and passenger rail lines, a shipping port, and suburban residences (see map in Figure S5).
Grab samples of ambient air were collected between 10:00 AM to 12:00 PM to characterize the daytime O₃ formation
rates in the presence of variable atmospheric mixing and regional emissions. Sensitivities were based on perturbation
190 concentrations of approximately 8 ppb of NO_x injected into chamber #1 and 8 ppb of VOC surrogates injected into
chamber #3. Initial gas concentrations were measured from the full chambers in the dark over a 30 min period (10 min
for each chamber). The UV lamp panels were then illuminated for 180 min and the chamber concentrations were
measured in a continuous cycle of 10 min intervals over a total of seven cycles. Each active monitoring period lasted
195 each chamber averaged in each 10 min sampling interval increased linearly over the 180 min period when the UV
lights were on. A linear regression model was therefore applied to extrapolate O₃ concentrations in each chamber to
the end of the measurement period to facilitate direct comparisons between the basecase chamber #2 and perturbed
chambers #1 and #3. O₃ concentration after 3-hour UV exposure were estimated for each chamber based on the linear
regression model. The difference of O₃ concentration after 3-hour UV exposure was calculated between chamber #1
200 to chamber #2 ($\Delta O_3^{+NO_x}$), and chamber #3 to chamber #2 ΔO_3^{+VOC} to quantify the O₃ sensitivity.

3. Results

3.1 Chamber measurement and satellite results in Sacramento

3.1.1 Monthly variation of ambient gas concentrations

205 Figure 2 compares the ground-based measurements and the TROPOMI column measurements of NO_x and VOC
surrogate concentrations at the Sacramento sampling site. Good agreement is observed between the time trends of the
chamber and TROPOMI satellite remote sensing measurements. Both techniques identify strong seasonal patterns for
the concentrations of the O₃ precursors.

210 Figure 2a shows the monthly averaged TROPOMI satellite NO₂ measurements and the boxplot of daily chamber NO₂
measurements at Sacramento between February – December 2020. NO₂ concentrations remained relatively stable
between April and July and then sharply increase in August – September possibly due to increased wildfires in the
late summer months. Enrichment of NO₂ and other pollutants in wildfire plumes has been noted in previous research
(Jaffe and Wigder, 2012). The open boxes in Figure 2a represent days within the months of August – November that
were not influenced by wildfire smoke (Rohrbacher and Kuwayama, n.d.), leading to reduced NO₂ concentrations.
215 The upward trend in NO₂ concentrations in October – December, 2020 is likely associated with decreased boundary



layer heights and increased fuel consumption for heating during the colder fall – winter season. This seasonal association can also be viewed in the decreasing TROPOMI satellite NO₂ levels measured during the warmer spring season (February – April, 2020). The effects of reduced transportation emissions in March – April, 2020 caused by COVID-19 shelter-in-place orders are notably minor in the ambient NO₂ measurements. Although light-duty vehicle traffic decreased by as much as 50% during this time period, heavy-duty truck traffic was more constant (Liu et al., 2020; Parker et al., 2020). The ground-based measurement site is 0.8 and 1.8 km from two major freeways, but NO_x concentrations at this site do not appear to be strongly influenced by the COVID-19 reduction in light-duty traffic activity. Increasing NO_x emissions from residences and relatively quick recovery of the heavy-duty traffic compared to the light-duty traffic may also minimize COVID-19 effects on NO_x concentrations (Liu et al., 2021). The seasonal pattern of NO_x concentrations driven by wildfires, reduced boundary layer height, and increased residential fuel consumption appears to dominate at the urban Sacramento location.

Figure 2b shows the monthly averaged TROPOMI satellite HCHO levels and the daily ground-based CO*Biogenic concentration at the Sacramento sampling site. The agreement between the seasonal trend in the CO*Biogenic and TROPOMI HCHO builds confidence in the use of CO*Biogenic as a ground-based indicator of VOC concentrations at this location. Both indicators suggest that VOC concentrations increased from April – August 2020, and sharply declined in October 2020. Wildfires can emit large amounts of VOCs that can be transported to urban areas (Zhang et al., 2018). It is possible that wildfires contributed to the highest VOC concentrations observed between August and September 2020. Removing the days influenced by wildfires (open box) still leaves a strong seasonal trend with increasing VOC concentrations between April – August 2020, which is consistent with increasing VOC emissions from biogenic sources. Biogenic VOC (BVOC) emissions increase during warmer spring months and continue to increase as temperatures rise into summer (Guenther et al., 2006, 1991). The CO*Biogenic factor inherently incorporates this effect, but the strong agreement between the TROPOMI HCHO levels and the CO*biogenic metric in Figure 2b suggests that the seasonal pattern of the biogenic emissions is a real feature of the dataset and not an artifact of how the CO*biogenic metric was constructed. Similarly, the declining VOC concentration observed in October, 2020 and beyond, matched the expected decrease of biogenic emissions during the colder fall and winter seasons when vegetation becomes dormant. The seasonal pattern illustrated in Figure 2b suggests that BVOC is an important precursor of HCHO in Sacramento.

PAMS measurements of ground-level isoprene concentrations in Sacramento are shown as blue diamonds in Figure 2b. Isoprene is highly reactive in the atmosphere and so PAMS measured concentrations are lower than 4 ppb. The limited time period of available measurements makes it difficult to discern seasonal trends, but the slightly lower measured isoprene concentrations in July, slightly higher isoprene concentrations in August followed by decreasing (non-wildfire) isoprene concentrations in September generally match the VOC trends generated using both TROPOMI HCHO and CO*Biogenic. Once again, the agreement between the three independent techniques builds confidence in the overall assessment of VOC seasonal trends.



255 Volatile chemical products (VCP) are another important category of VOCs emissions (McDonald et al., 2018). The expanded usage of spray disinfectant and sanitization products during the COVID-19 pandemic might have been a significant source of VOCs in the urban area, but the expected usage pattern of these products does not include a sharp decline in the fall period. The seasonal pattern of VOC concentrations increasing during spring – summer and decreasing during fall – winter is more consistent with a combination of biogenic sources and wildfires, as discussed above.

3.1.2 Seasonal trends in O₃ sensitivity

260 Figure 3a shows the monthly trends in measured $\Delta O_3^{+NO_x}$ and TROPOMI HCHO/NO₂ from February 2020 to December 2020 at the Sacramento site. The $\Delta O_3^{+NO_x}$ value represents the change in O₃ concentrations in response to a +8 ppb NO_x perturbation. O₃ formation is NO_x-limited when the $\Delta O_3^{+NO_x}$ value is positive, and VOC-limited when the $\Delta O_3^{+NO_x}$ value is negative. Changes in the absolute magnitudes of the $\Delta O_3^{+NO_x}$ values reflect the degree of O₃ sensitivity to the NO_x perturbation. $\Delta O_3^{+NO_x}$ and TROPOMI HCHO/NO₂ both increase from April to August 2020, and then sharply decline in October 2020. By comparing the transition points of $\Delta O_3^{+NO_x} = 0$ and TROPOMI HCHO/NO₂ = 4.6 (discussed in Section 3.2), it is evident that O₃ formation evolved from VOC-limited conditions in spring towards NO_x-limited conditions from June to August, followed by a return to VOC-limited conditions after October 2020. It is notable that the seasonal trend for $\Delta O_3^{+NO_x}$ matches the trend of increased BVOC emissions during the summer and increased NO_x emissions during the winter. The travel restrictions associated with COVID-19 that occurred in March – May 2020, appeared to have little impact on the overall seasonal trends in $\Delta O_3^{+NO_x}$ behavior.

275 The median ground-based $\Delta O_3^{+NO_x} < 0$ indicates VOC-limited conditions in September 2020, but the TROPOMI satellite HCHO/NO₂ > 4.6 indicates NO_x-limited conditions for this same month. Removing the wildfire days from the analysis period (open box in Figure 3a) did not reconcile the two measurements. The divergence of the ground-based measurements and satellite measurements in this month may reflect the presence of elevated plumes of wildfire smoke above the monitoring site that were detected by the satellite measurements (Jin et al., 2017). Cleaner air at the ground-based monitors, therefore, yielded $\Delta O_3^{+NO_x}$ values in a different chemical regime than the satellite measurements that are based on the tropospheric vertical column densities. This comparison suggests that ground-based measurements may be required to supplement satellite-based measurements to fully characterize the surface O₃ formation regime under special circumstances that generate concentrated pollution layers above the ground-level.

285 Removing the days influenced by wildfires from the chamber measurement (open box) and TROPOMI satellite measurement (open diamond) in Figure 3a reduces both $\Delta O_3^{+NO_x}$ and TROPOMI HCHO/NO₂. The comparison between wildfire vs. non-wildfire days implies that wildfires emit more VOC than NO_x, which is in agreement with previous studies (Jaffe and Wigder, 2012). It is also notable that the decrease of $\Delta O_3^{+NO_x}$ is larger than the decrease in TROPOMI HCHO/NO₂. This observation might once again reflect the fact that the wildfire identification algorithm



(Rohrbacher and Kuwayama, n.d.) was based on ground-level measurements that do not flag all of the days with elevated plumes above the monitoring site that could differentially affect the satellite measurements.

290 Figure 3b shows the monthly variation of ground-based ΔO_3^{+VOC} and TROPOMI satellite HCHO/NO₂ February –
December 2020, at the Sacramento sampling site. ΔO_3^{+VOC} (Figure 3b) has an inverse time trend compared to $\Delta O_3^{+NO_x}$
and TROPOMI HCHO/NO₂ (Fig 2a). The ΔO_3^{+VOC} trend is well-correlated to the TROPOMI HCHO/NO₂ trend plotted
on a reversed axis between April – August 2020, but the two trends diverge in September – October 2020 when
wildfires were prevalent. Removing the wildfire days from August to October (open box) increased the ground-based
295 ΔO_3^{+VOC} , once again suggesting that wildfires contributed more VOCs than NO_x to the atmosphere (Altshuler et al.,
2020). The divergence between the ground-based ΔO_3^{+VOC} measurements and TROPOMI satellite HCHO/NO₂
measurements during the wildfire season once again reflects the presence of elevated plumes that were measured by
the satellite but not by the ground-based monitors (Schroeder et al., 2017).

3.1.3 Weekend effect

300 Figure 4 separately plots concentrations of O₃ precursors and O₃ sensitivity on weekdays (shaded bars) and weekends
(open bars) during the current study period. Direct wildfire days have been removed from the analysis (Rohrbacher
and Kuwayama, n.d.) to focus on the day-of-week patterns. Hypothesis tests were carried out to determine if weekday
and weekend responses were similar in each month. The results indicate that weekend reductions in NO₂
concentrations were significant at a 90% confidence level (or higher) before July. The similarity between weekday
305 and weekend NO₂ concentrations after July may be associated with increased NO_x emissions from wildfires in the late
summer and space heating in the fall – winter since neither of these sources follows a weekday/weekend pattern.
Although days directly affected by the wildfire smoke were removed from the analysis, residual emissions from
smoldering fires and multi-day recirculation of air mass that have been affected by wildfire smoke may have
contributed to elevated regional NO_x concentrations through the formation of reactive nitrogen reservoir species such
310 as peroxyacetyl nitrate (PAN) that can be transported over long distances (Lindaas et al., 2017). The CO*Biogenic
VOC surrogate did not display statistically significant differences between weekdays vs. weekends except in June and
July. Extremely hot days (> 35°C) occurred on weekdays in June and weekends in July, driving the CO*Biogenic
factor higher.

315 Reduced NO_x emissions on weekends are reflected in the O₃ sensitivity to precursors shown in Figure 4c and d. The
median $\Delta O_3^{+NO_x}$ sensitivity is higher on weekends for most months indicating that the atmosphere was more NO_x-
limited. Large variability in the data makes the weekend vs. weekday $\Delta O_3^{+NO_x}$ response statistically significant at the
90% (or higher) level only in April, September, and October. The large weekend reductions in median NO₂
concentrations detected in May and June did not lead to significantly higher weekend $\Delta O_3^{+NO_x}$, possibly because of
320 higher weekday median VOC concentrations in these months. Median O₃ sensitivity was NO_x-limited ($\Delta O_3^{+NO_x} > 0$)
on both weekdays and weekends from June to August when BVOC emissions are expected to be highest. In spring



and early fall (April, May and September), the median weekday O₃ sensitivity is VOC-limited but the median weekend O₃ sensitivity is NO_x-limited. In late fall and winter (October ~ November), the median O₃ sensitivity is VOC-limited on both weekends and weekdays. Weekend NO_x reductions have an inverse effect on ΔO_3^{+VOC} shown in Figure 4d compared to $\Delta O_3^{+NO_x}$. The median ΔO_3^{+VOC} is lower on weekends than weekdays because the O₃ formation is more NO_x-limited on weekends.

3.1.4 O₃ isopleth measurements

Figure 5 summarizes the NO_x, CO*Biogenic, O₃, $\Delta O_3^{+NO_x}$, and ΔO_3^{+VOC} measurements in Sacramento from April to December in 2020 in the format of an O₃ isopleth diagram. Each data point in Figure 5 corresponds to measurements on a single day. The color of each symbol represents the O₃ concentration in the baseline chamber (no NO_x or VOC perturbation) after 3-hours of UV irradiation. The NO_x and CO*Biogenic scale factors are relative to the NO_x and CO*biogenic levels measured on the day with the mean O₃ concentration. The arrow attached to each data symbol points in the direction of maximum ΔO_3 in response to NO_x and VOC addition. The magnitude of the arrow corresponds to the strength of the ΔO_3 response. All arrows generally point right, meaning that VOC addition increased O₃ concentrations. Arrows pointing to the bottom right indicate that NO_x addition decreased the O₃ concentration, while arrows pointing to the upper right indicate that NO_x addition increased the O₃ concentrations. The most effective emissions control program acts in the direction opposite to each arrow.

The mixture of daily data points (yellow to red points) shows the O₃ isopleth pattern where higher O₃ concentration (darker color) exists at higher NO_x and VOC concentrations. The combination of the colors and the arrows illustrated in the isopleth diagram help to define the measured “ridgeline” in the O₃ isopleth diagram that denotes the transition between VOC-limited chemistry and NO_x-limited chemistry at Sacramento. Arrows in the upper left of the diagram point downwards (VOC-limited) towards the ridgeline, while arrows in the lower right of the diagram point upwards (NO_x-limited) towards the ridgeline. The atmospheric system experiences a range of conditions throughout the nine-month study period that moved the measurements around the O₃ isopleth diagram. The average seasonal cycle is illustrated in Figure 5 using monthly-average points shown as blue circles with white month numbers. The monthly-average O₃ chemical regime traces an oval path through the isopleth diagram as NO_x concentrations decrease and CO*Biogenic (proxy of VOC) concentrations increase moving from spring to summer months. NO_x concentrations increase rapidly in fall while CO*Biogenic concentrations simultaneously decrease at the Sacramento sampling location, transitioning the O₃ chemistry to VOC-limited conditions. The pattern is expected to reverse for the months of January – March (not shown) to produce a repeatable annual cycle. The direct measurement of the seasonal pattern of the O₃ chemical regime clearly illustrates the effects of NO_x and VOC emissions controls at different times of the year.

3.1.5 Extreme value analysis for O₃ sensitivity

The days with the high measured O₃ concentrations are of particular interest in the current study since emissions control programs are traditionally tailored to reduce peak O₃ concentrations, not monthly-average O₃ concentrations.



Figure 6 illustrates box-and-whisker plots of measured $\Delta O_3^{+NO_x}$, and ΔO_3^{+VOC} at Sacramento binned according to the maximum O_3 concentration in the basecase chamber on the x-axis. Days influenced by wildfires were removed from the analysis in order to focus on the “routine” O_3 formation dynamics. The five bins corresponding to the highest O_3 concentrations (≥ 80 ppb) have median O_3 sensitivity in the NO_x -limited regime where NO_x addition increases O_3 concentrations and VOC addition has minor effects on O_3 concentrations, suggesting that a NO_x emissions control strategy would be most effective at reducing these peak O_3 concentrations. In contrast, days with O_3 concentrations just below 80 ppb had median O_3 sensitivity that was VOC-limited, suggesting that an emissions control strategy focusing on NO_x reduction would increase O_3 concentrations. VOC controls on these intermediate days would be difficult, however, if biogenic VOCs account for the majority of the O_3 formation. This challenging situation suggests that emissions control programs that focus on NO_x reductions will immediately lower peak O_3 concentrations, but slightly increase intermediate O_3 concentrations until NO_x levels fall far enough to re-enter the NO_x -limited regime.

Additional statistical analysis was carried out to characterize the extreme values in the O_3 sensitivity plots (Coles, 2001; Gilleland and Katz, 2016). Extreme value analysis characterizes high concentrations using “return levels” corresponding to a specified time period (T). In the context of the current analysis, the return level is the ΔO_3 perturbation response that is expected to be exceeded once during the specified time period. The probability of exceeding the return level is therefore $1/T$. Figure 7 shows the 90-day return level for $\Delta O_3^{+NO_x}$ and ΔO_3^{+VOC} sensitivity based on statistical analysis of the measured perturbation response in each month. The 90-day time period was chosen to correspond to the time period inherent in the O_3 design value values that are based on the annual 4th highest O_3 concentration averaged in three years (12 “exceedances” / 1095 days equals approximately one “exceedance” / 90 days). The 90-day return value of O_3 sensitivity can therefore be viewed as the design value for O_3 sensitivity. Figure 7 shows that the 90-day return levels for O_3 sensitivity and the median O_3 sensitivity follow similar seasonal trends, but the extreme values are shifted higher such that they are NO_x -limited from April to December, except November which is slightly VOC-limited. The positive 90-day return levels of $\Delta O_3^{+NO_x}$ once again suggest the NO_x control is an efficient strategy to reduce peak O_3 concentrations in Sacramento.

3.2 Chamber and TROPOMI data correlation

The consistency between the NO_x and VOC measurements made using ground-based chambers and satellite observations enables a joint analysis to directly calculate the TROPOMI HCHO/ NO_2 ratio at the transition between NO_x and VOC limited O_3 formation regimes. Three circular buffers (2.5, 5, and 7.5 km radii) centered on the monitoring location were used to generate the TROPOMI HCHO/ NO_2 ratio that was then compared to the measured $\Delta O_3^{+NO_x}$ ratio at the monitoring site. The HCHO/ NO_2 ratio generated using the 5 km radius buffer shows the best correlation with ground-based chamber results shown in Figure 8a (results from other buffers are shown in Figure S6). Linear regression analysis between 1-week-averaged $\Delta O_3^{+NO_x}$ and HCHO/ NO_2 with and without wildfires shows that removing the wildfires always improves the correlation coefficient (R), likely because the elevated wildfire plumes have different effects on surface vs. integrated column measurements. The regression carried out using a 5 km buffer radius with wildfires removed yielded a correlation coefficient $R = 0.62$ ($p < 0.001$). The transition point between



NO_x-limited and VOC-limited conditions (corresponding to $\Delta O_3^{+NO_x} = 0$) occurs when HCHO/NO₂ = 4.6 (95% confidence interval: 4.39 ~ 5.90). When the TROPOMI satellite HCHO/NO₂ ratio fell below 4.6 then the ground-based measurement of $\Delta O_3^{+NO_x}$ was usually negative, and when the satellite HCHO/NO₂ ratio rose above 4.6 then the ground-based measurement of $\Delta O_3^{+NO_x}$ was usually positive. This direct measurement of the HCHO/NO₂ transition point is consistent with previous estimates constructed from the combination of satellite measurements and routine ground-based O₃ monitoring data (Jin et al., 2020).

3.3 TROPOMI O₃ sensitivity in California

Figure 9 displays the monthly-average spatial distribution of TROPOMI HCHO/NO₂ ratios across California for the time period April – October, 2020. Overall, TROPOMI HCHO/NO₂ was the lowest (mean (Standard deviation) = 3.5 (1.2)) in April and the highest (mean (standard deviation) = 9.7 (3.2)) in July. The seasonal pattern of increasing NO_x limitation during the summer months at Sacramento (Figure 3a, b) is mirrored across most of California (Figure 9), especially in the mountainous areas with dense vegetation. The majority of California is in the VOC-limited regime in April and May due to the low BVOC emissions. Only very remote regions with low NO_x concentrations are still in the NO_x-limited regime during these spring months. Most areas outside of major urban centers transition toward NO_x-limited conditions between June and September as ambient temperature and BVOC emissions increase. These areas then transition back to the VOC-limited regime in the fall months beginning in October as temperatures decrease and vegetation becomes dormant.

Large urban centers including Los Angeles, San Diego, and the San Francisco Bay Area exhibit low HCHO/NO₂ ratios (VOC-limited conditions) throughout the study period. These urban areas contain less vegetation and larger numbers of NO_x sources than outlying suburban and rural areas. Therefore, reducing NO_x emissions in these urban centers may increase monthly-average O₃ concentrations throughout the year. The HCHO/NO₂ ratio in California's Central Valley is lower than the HCHO/NO₂ ratio in the surrounding mountainous area during all months of the study period. This spatial pattern reflects the high BVOC emissions from coniferous forests in the mountainous regions compared to the cropland in the Central Valley (Miszta et al., 2014).

Past studies have found that wildfire smoke plumes mixing with high urban NO_x emissions can lead to enhanced urban O₃ concentrations (Jaffe and Wigder, 2012). The effects of wildfires during August – September 2020, can be observed in Figure 9 as zones of reduced HCHO/NO₂ immediately around the active burn areas followed by a larger “halo” zone of increased HCHO/NO₂ as the VOCs emitted from wildfires have time to react to form HCHO. This “halo” pattern is most obvious in October 2020, when the seasonal cycle of biogenic emissions declined sufficiently to shift the O₃ sensitivity back to the VOC-limited regime for the majority of the state except for the region surrounding a wildfire in the Sierra Nevada mountain range east of Fresno (near Yosemite National Park). VOCs emitted from the wildfire in October 2020, reacted to produce HCHO in the “halo” region, keeping the HCHO/NO₂ ratio in the NO_x-limited regime. The extensive wildfires that occurred in 2020 appear to have extended the natural peak of the HCHO/NO₂ ratio from July into August, September, and even October 2020. It is unknown whether this satellite



430 observation accurately represents conditions at ground level. The results at the Sacramento monitoring site in
September 2020 (Figure 3a and b) suggest that elevated smoke plumes can dominate the satellite observations, but
they may not accurately represent conditions at ground level.

435 Figure 10 illustrates the monthly-average TROPOMI HCHO/NO₂ ratio over the period February – October 2020, for
seven air basins in California that include 8-hour O₃ NAAQS nonattainment areas. The HCHO/NO₂ ratio in all seven
air basins sharply rises in late spring and reaches a peak in June – July. The HCHO/NO₂ ratios in the SoCAB and San
Diego County steadily decline in the months between July and October. In contrast, the air basins in central and
Northern California that were more heavily impacted by wildfires exhibit a second peak in the HCHO/NO₂ ratio in
September, possibly due to the smoke plumes mixing into the regional air. Similar seasonal patterns are observed for
all the air basins in California (Table S1). The patterns illustrated in Figure 10 are consistent with BVOC emissions
440 cycles combined with wildfire effects in California.

The SoCAB had the lowest HCHO/NO₂ ratio among all the air basins in California during the study period. This is
noteworthy since the SoCAB has the highest population and the highest O₃ concentrations. The San Francisco Bay
Area and San Diego County, two other heavily populated areas in California, also have relatively low HCHO/NO₂
445 ratios compared to other air basins. Using HCHO/NO₂ = 4.6 as the transition point, even these highly urbanized air
basins appear to transition from VOC-limited to NO_x-limited O₃ formation chemistry in summer 2020. It is
noteworthy, however, that the urban cores of these regions remain VOC-limited across all months due to very high
NO_x emissions (see persistently green regions in Figure 9). Thus, the optimal emissions control strategy for the entire
air basin may differ from the optimal emissions control strategy for urban cores areas.

450 **4. Discussion**

California's O₃ control strategies mainly focus on NO_x emissions from motor vehicles (William and Burke, 2016) and
especially heavy-duty trucks (Burke, 2020). Additional control strategies would require cleaner engines and zero /
near-zero emission technologies (Brown, 2018; South Coast AQMD, 2021). VOC sources that dominate O₃ formation
are still not clear due to the large numbers of activities that release VOCs and the complex reactions that VOCs
455 undergo in the atmosphere. Controls on VOC emissions have been more effective than controls on NO_x emissions
over the past decades, mainly because of reduced emissions from large stationary sources (Barcikowski et al., 2017).
VOC emissions decreased by a factor of 3 while NO_x emissions decreased by a factor of 1.5 between 1980 to 2010
(Cox et al., 2013; Rasmussen et al., 2013). Recent studies have shown that VOCs from consumer products are
underestimated in the emission inventory (McDonald et al., 2018). However, the clear seasonal pattern in the measured
460 O₃ sensitivity and the corresponding pattern for concentrations of VOC proxies (HCHO and CO*Biogenic) suggests
that BVOCs are also important.



465 The 2016 California State Implementation Plan calls for a 34% reduction in NO_x emissions and a 30% reduction in
VOC emissions (California Air Resources Board, 2018), which will increase the VOC/NO_x ratio. This will reduce
peak O₃ concentrations in most areas across California that become NO_x-limited in the middle of the summer. In
contrast, the NO_x emissions control program could cause a short-term increase in peak O₃ concentrations in the urban
cores that are currently VOC-limited and it could increase intermediate O₃ concentrations in late spring or early fall
as regions transition back to VOC-limited conditions. These regions do not currently violate the O₃ NAAQS, but they
could experience future violations depending on the timing of the transition to lower NO_x concentrations. Despite
470 these penalties, controls on NO_x emissions may be the only alternative for long-term O₃ reductions in regions where
VOC emissions are dominated by biogenic sources. As the NO_x keeps decreasing, the O₃ photochemical regime will
eventually transition back to NO_x-limited conditions and all further NO_x reductions will yield decreasing O₃
concentrations. Previous studies have observed such a transition between VOC-limited to NO_x-limited conditions in
polluted urban areas with high NO_x concentrations. Jin et al. (2020) observed a suppression of the NO_x-limited area
475 between 2013 – 2016 vs. 1996 – 2000 in Los Angeles by analysing satellite HCHO/NO₂ ratios. Baidar et al. (2015)
observed a weakening of the higher O₃ concentrations on weekends in the SoCAB between 1996 to 2014, reflecting
a transition towards more NO_x-limited conditions. These studies suggest that continued reductions in NO_x emissions
will eventually yield a transition to fully NO_x-limited conditions in Los Angeles, albeit this transition may not be fully
complete for decades.

480

Wildfires are an unpredictable factor that enhances O₃ formation in California. O₃ formation during wildfire events
shifts towards more NO_x-limited conditions, making reductions in NO_x emissions attractive. The frequency and scale
of wildfires in the western U.S. have increased over time due to the effects of drought and climate change (U.S.
Global Change Research Program, 2018). Abatement strategies may focus on wildfire prevention as an effective way
485 to reduce incidental O₃ concentrations.

5. Conclusion

Direct measurements of O₃ sensitivity to precursor NO_x and VOC concentrations using a mobile smog chamber system
in Sacramento, CA from April to December, 2020 show that O₃ sensitivity follows a seasonal cycle. O₃ formation is
VOC-limited in the spring, NO_x-limited in the summer, and returns to VOC-limited in fall – winter. This seasonal
490 pattern reflects higher emissions of reactive VOCs during the summer season and increased NO_x concentrations during
the other seasons. The most obvious potential source of increased VOC emissions during the summer season is
biogenics. Comparing the ground-based chamber measurements to satellite measurements from TROPOMI suggests
that the transition between NO_x-limited and VOC-limited chemical regimes for O₃ formation occurs at a TROPOMI
HCHO/NO₂ ratio of 4.6. Monthly-averaged TROPOMI measurements show that O₃ sensitivity across most of
495 California follows a seasonal cycle similar to Sacramento, but locations with higher population density are more VOC-
limited. The urban cores of most large cities remain VOC-limited in all seasons even when the surrounding areas
become NO_x-limited in the middle of summer. The variability of the chemical regime for O₃ formation across space
and time makes it difficult to design an emissions control strategy that will equitably reduce O₃ concentrations for all



500 California residents currently living in air basins that violate the 8-hour O₃ NAAQS. Reductions in NO_x emissions
will be the most efficient control strategy to reduce present-day peak O₃ concentrations, but this strategy will lead to
increasing O₃ concentrations in urban cores during the middle of summer and increasing O₃ concentrations in
surrounding regions during late spring and early fall. These penalties will persist until NO_x emissions are reduced
sufficiently to push the entire region into NO_x-limited conditions sometime in the coming decades. VOC emissions
505 reductions never cause increasing O₃ concentrations and O₃ formation is VOC-limited during some seasons. It may
be advisable to augment NO_x emissions control programs with some amount of controls on volatile consumer products
(VCPs) and mitigation of wildfires in an attempt to reduce any near-term increases in O₃ concentrations. Continued
deep NO_x emissions reductions should eventually transition all locations across California into the NO_x-limited
regime, and will effectively push the state toward 8-hour O₃ NAAQS attainment

Acknowledgment:

510 The authors thank Michael Miguel, Anthony Esparza, and Aimee Davis of the California Air Resources Board
(CARB) for their logistical support surrounding the siting of the chamber experiments. Part of this study was supported
by CARB Agreement No. 19RD012 and Coordinated Research Council (CRC) Agreement No. A-121. The views
expressed in this article are those of the authors and do not represent the views or policies of CARB.

References

- 515 Altshuler, S. L., Zhang, Q., Kleinman, M. T., Garcia-Menendez, F., Moore, C. T., Hough, M. L., Stevenson, E. D.,
Chow, J. C., Jaffe, D. A. and Watson, J. G.: Wildfire and prescribed burning impacts on air quality in the United
States, *J. Air Waste Manag. Assoc.*, 70(10), 961–970, doi:10.1080/10962247.2020.1813217, 2020.
American Lung Association: The State of the Air 2019. [online] Available from: <https://www.lung.org/media/press-releases/state-of-the-air-california> (Accessed 15 March 2021), 2020.
- 520 Baidar, S., Hardesty, R. M., Kim, S. W., Langford, A. O., Oetjen, H., Senff, C. J., Trainer, M. and Volkamer, R.:
Weakening of the weekend ozone effect over California's South Coast Air Basin, *Geophys. Res. Lett.*, 42(21), 9457–
9464, doi:10.1002/2015GL066419, 2015.
Baker, A. K., Beyersdorf, A. J., Doezema, L. A., Katzenstein, A., Meinardi, S., Simpson, I. J., Blake, D. R. and
Sherwood Rowland, F.: Measurements of nonmethane hydrocarbons in 28 United States cities, *Atmos. Environ.*,
525 42(1), 170–182, doi:10.1016/j.atmosenv.2007.09.007, 2008.
Barcikowski, W., Cheung, K., Cohan, S., Durkee, K., Eckerle, E., Epstein, S., Farina, S., Farr, H., Trainor Gamino,
K., Ghasemi, A., Katzenstein, A., Kang, E., Laybourn, M., Lee, J. H., Lee, S.-M., Orellana, K., Pakbin, P., Sospedra,
M. C., Thai, D. and Zhang, X.: Final 2016 Air Quality Management Plan. [online] Available from:
<http://www.aqmd.gov/home/air-quality/clean-air-plans/air-quality-mgt-plan/final-2016-aqmp> (Accessed 3 May
530 2021), 2017.
Brown, E. G.: Zero-Emission Vehicles (ZEV) Action Plan 2018 updated. [online] Available from: www.cecsb.org
(Accessed 12 May 2021), 2018.



- Burke, W.: South Coast Air Quality Management District Annual report 2019, Diamond Bar, CA., 2020.
- California Air Resources Board: California Ambient Air Quality Standards, [online] Available from:
535 <https://ww2.arb.ca.gov/resources/california-ambient-air-quality-standards> (Accessed 1 April 2021), 2007.
- California Air Resources Board: 2018 Updates to the California State Implementation Plan. [online] Available from:
<https://ww2.arb.ca.gov/resources/documents/2018-updates-california-state-implementation-plan-2018-sip-update>
(Accessed 12 May 2021), 2018.
- Carter, W., Luo, D., Malkina, I. and Pierce, J.: Environmental Chamber Studies of Atmospheric Reactivities of
540 Volatile Organic Compounds: Effects of Varying Chamber and Light Source, , doi:10.2172/57153, 1995.
- Chen, S. P., Liu, T. H., Chen, T. F., Yang, C. F. O., Wang, J. L. and Chang, J. S.: Diagnostic modeling of PAMS VOC
observation, *Environ. Sci. Technol.*, 44(12), 4635–4644, doi:10.1021/es903361r, 2010.
- Coles, S.: An Introduction to Statistical Modeling of Extreme Values, Springer London, London., 2001.
- Cox, P., Delao, A. and Komorniczak, A.: The California Almanac of Emissions and Air Quality - 2013 Edition.
545 [online] Available from: <https://www.arb.ca.gov/aqd/almanac/almanac13/almanac13.htm>, 2013.
- Duncan, B. N., Yoshida, Y., Olson, J. R., Sillman, S., Martin, R. V., Lamsal, L., Hu, Y., Pickering, K. E., Retscher,
C., Allen, D. J. and Crawford, J. H.: Application of OMI observations to a space-based indicator of NO_x and VOC
controls on surface ozone formation, *Atmos. Environ.*, 44(18), 2213–2223, doi:10.1016/j.atmosenv.2010.03.010,
2010.
- 550 Van Geffen, J., Folkert Boersma, K., Eskes, H., Sneep, M., Ter Linden, M., Zara, M. and Pepijn Veefkind, J.: S5P
TROPOMI NO₂ slant column retrieval: Method, stability, uncertainties and comparisons with OMI, *Atmos. Meas.
Tech.*, 13(3), 1315–1335, doi:10.5194/amt-13-1315-2020, 2020.
- Gilleland, E. and Katz, R. W.: ExtRemes 2.0: An extreme value analysis package in R, *J. Stat. Softw.*, 72(1), 1–39,
doi:10.18637/jss.v072.i08, 2016.
- 555 Guenther, A., Karl, T., Harley, P., Wiedinmyer, C., Palmer, P. I. and Geron, C.: Estimates of global terrestrial isoprene
emissions using MEGAN (Model of Emissions of Gases and Aerosols from Nature), *Atmos. Chem. Phys.*, 6(11),
3181–3210, doi:10.5194/acp-6-3181-2006, 2006.
- Guenther, A. B., Monson, R. K. and Fall, R.: Isoprene and monoterpene emission rate variability: Observations with
eucalyptus and emission rate algorithm development, *J. Geophys. Res.*, 96(D6), 10799, doi:10.1029/91jd00960, 1991.
- 560 Howard, C. J., Yang, W., Green, P. G., Mitloehner, F., Malkina, I. L., Flocchini, R. G. and Kleeman, M. J.: Direct
measurements of the ozone formation potential from dairy cattle emissions using a transportable smog chamber,
Atmos. Environ., 42(21), 5267–5277, doi:10.1016/j.atmosenv.2008.02.064, 2008.
- Howard, C. J., Kumar, A., Malkina, I., Mitloehner, F., Green, P. G., Flocchini, R. G. and Kleeman, M. J.: Reactive
organic gas emissions from livestock feed contribute significantly to ozone production in central California, *Environ.*
565 *Sci. Technol.*, 44(7), 2309–2314, doi:10.1021/es902864u, 2010.
- Ialongo, I., Virta, H., Eskes, H., Hovila, J. and Douros, J.: Comparison of TROPOMI/Sentinel-5 Precursor NO₂
observations with ground-based measurements in Helsinki, *Atmos. Meas. Tech.*, 13(1), 205–218, doi:10.5194/amt-
13-205-2020, 2020.
- Jacob, D. J. and Winner, D. A.: Effect of climate change on air quality, *Atmos. Environ.*, 43(1), 51–63,



- 570 doi:10.1016/j.atmosenv.2008.09.051, 2009.
Jaffe, D. A. and Wigder, N. L.: Ozone production from wildfires: A critical review, *Atmos. Environ.*, 51, 1–10,
doi:10.1016/j.atmosenv.2011.11.063, 2012.
Jin, X., Fiore, A. M., Murray, L. T., Valin, L. C., Lamsal, L. N., Duncan, B., Folkert Boersma, K., De Smedt, I., Abad,
G. G., Chance, K. and Tonnesen, G. S.: Evaluating a Space-Based Indicator of Surface Ozone-NO_x-VOC Sensitivity
575 Over Midlatitude Source Regions and Application to Decadal Trends, *J. Geophys. Res. Atmos.*, 122(19), 10439–
10461, doi:10.1002/2017JD026720, 2017.
Jin, X., Jin, X., Fiore, A., Fiore, A., Boersma, K. F., Boersma, K. F., Smedt, I. De and Valin, L.: Inferring Changes in
Summertime Surface Ozone-NO_x-VOC Chemistry over U.S. Urban Areas from Two Decades of Satellite and
Ground-Based Observations, *Environ. Sci. Technol.*, 54(11), 6518–6529, doi:10.1021/acs.est.9b07785, 2020.
- 580 Jing, P., Lu, Z. and Steiner, A. L.: The ozone-climate penalty in the Midwestern U.S., *Atmos. Environ.*, 170, 130–
142, doi:10.1016/j.atmosenv.2017.09.038, 2017.
Jorga, S. D., Kaltsonoudis, C., Liangou, A. and Pandis, S. N.: Measurement of Formation Rates of Secondary Aerosol
in the Ambient Urban Atmosphere Using a Dual Smog Chamber System, *Environ. Sci. Technol.*, 54(3), 1336–1343,
doi:10.1021/acs.est.9b03479, 2020.
- 585 Kleinman, L. I.: The dependence of tropospheric ozone production rate on ozone precursors, *Atmos. Environ.*, 39(3),
575–586, doi:10.1016/j.atmosenv.2004.08.047, 2005.
Kroll, J. H., Heald, C. L., Cappa, C. D., Farmer, D. K., Fry, J. L., Murphy, J. G. and Steiner, A. L.: The complex
chemical effects of COVID-19 shutdowns on air quality, *Nat. Chem.*, 12(9), 777–779, doi:10.1038/s41557-020-0535-
z, 2020.
- 590 Lafranchi, B. W., Goldstein, A. H. and Cohen, R. C.: Observations of the temperature dependent response of ozone
to NO_x reductions in the Sacramento, CA urban plume, *Atmos. Chem. Phys.*, 11(14), 6945–6960, doi:10.5194/acp-
11-6945-2011, 2011.
Lindaas, J., Farmer, D. K., Pollack, I. B., Abeleira, A., Flocke, F., Roscioli, R., Herndon, S. and Fischer, E. V.:
Changes in ozone and precursors during two aged wildfire smoke events in the Colorado Front Range in summer
595 2015, *Atmos. Chem. Phys.*, 17(17), 10691–10707, doi:10.5194/acp-17-10691-2017, 2017.
Liu, J., Lipsitt, J., Jerrett, M. and Zhu, Y.: Decreases in Near-Road NO and NO₂ Concentrations during the COVID-
19 Pandemic in California, *Environ. Sci. Technol. Lett.*, (2), doi:10.1021/acs.estlett.0c00815, 2020.
Liu, Q., Harris, J. T., Chiu, L. S., Sun, D., Houser, P. R., Yu, M., Duffy, D. Q., Little, M. M. and Yang, C.:
Spatiotemporal impacts of COVID-19 on air pollution in California, USA, *Sci. Total Environ.*, 750,
600 doi:10.1016/j.scitotenv.2020.141592, 2021.
Martin, R. V., Fiore, A. M. and Van Donkelaar, A.: Space-based diagnosis of surface ozone sensitivity to
anthropogenic emissions, *Geophys. Res. Lett.*, 31(6), 2–5, doi:10.1029/2004gl019416, 2004.
McDonald, B. C., De Gouw, J. A., Gilman, J. B., Jathar, S. H., Akherati, A., Cappa, C. D., Jimenez, J. L., Lee-Taylor,
J., Hayes, P. L., McKeen, S. A., Cui, Y. Y., Kim, S. W., Gentner, D. R., Isaacman-VanWertz, G., Goldstein, A. H.,
605 Harley, R. A., Frost, G. J., Roberts, J. M., Ryerson, T. B. and Trainer, M.: Volatile chemical products emerging as
largest petrochemical source of urban organic emissions, *Science* (80-.), 359(6377), 760–764,



- doi:10.1126/science.aaq0524, 2018.
- Meng, Z., Dabdub, D. and Seinfeld, J. H.: Chemical coupling between atmospheric ozone and particulate matter, *Science* (80-.), 277(5322), 116–119, doi:10.1126/science.277.5322.116, 1997.
- 610 Misztal, P. K., Karl, T., Weber, R., Jonsson, H. H., Guenther, A. B. and Goldstein, A. H.: Airborne flux measurements of biogenic isoprene over California, *Atmos. Chem. Phys.*, 14(19), 10631–10647, doi:10.5194/acp-14-10631-2014, 2014.
- Nussbaumer, C. M. and Cohen, R. C.: The Role of Temperature and NO_x in Ozone Trends in the Los Angeles Basin, *Environ. Sci. Technol.*, 54(24), 15652–15659, doi:10.1021/acs.est.0c04910, 2020.
- 615 Parker, H. A., Hasheminassab, S., Crouse, J. D., Roehl, C. M. and Wennberg, P. O.: Impacts of Traffic Reductions Associated With COVID-19 on Southern California Air Quality, *Geophys. Res. Lett.*, 47(23), 1–9, doi:10.1029/2020GL090164, 2020.
- Parrish, D. D., Xu, J., Croes, B. and Shao, M.: Air quality improvement in Los Angeles—perspectives for developing cities, *Front. Environ. Sci. Eng.*, 10(5), doi:10.1007/s11783-016-0859-5, 2016.
- 620 Parrish, D. D., Young, L. M., Newman, M. H., Aikin, K. C. and Ryerson, T. B.: Ozone Design Values in Southern California’s Air Basins: Temporal Evolution and U.S. Background Contribution, *J. Geophys. Res. Atmos.*, 122(20), 11,166–11,182, doi:10.1002/2016JD026329, 2017.
- Pollack, I. B., Ryerson, T. B., Trainer, M., Parrish, D. D., Andrews, A. E., Atlas, E. L., Blake, D. R., Brown, S. S., Commane, R., Daube, B. C., De Gouw, J. A., Dubé, W. P., Flynn, J., Frost, G. J., Gilman, J. B., Grossberg, N., 625 Holloway, J. S., Kofler, J., Kort, E. A., Kuster, W. C., Lang, P. M., Lefer, B., Lueb, R. A., Neuman, J. A., Nowak, J. B., Novelli, P. C., Peischl, J., Perring, A. E., Roberts, J. M., Santoni, G., Schwarz, J. P., Spackman, J. R., Wagner, N. L., Warneke, C., Washenfelder, R. A., Wofsy, S. C. and Xiang, B.: Airborne and ground-based observations of a weekend effect in ozone, precursors, and oxidation products in the California South Coast Air Basin, *J. Geophys. Res. Atmos.*, 117(3), 1–14, doi:10.1029/2011JD016772, 2012.
- 630 Pusede, S. E. and Cohen, R. C.: On the observed response of ozone to NO_x and VOC reactivity reductions in San Joaquin Valley California 1995–present, *Atmos. Chem. Phys.*, 12(18), 8323–8339, doi:10.5194/acp-12-8323-2012, 2012.
- Pusede, S. E., Steiner, A. L. and Cohen, R. C.: Temperature and Recent Trends in the Chemistry of Continental Surface Ozone, *Chem. Rev.*, 115(10), 3898–3918, doi:10.1021/cr5006815, 2015.
- 635 Rasmussen, D. J., Hu, J., Mahmud, A. and Kleeman, M. J.: The ozone-climate penalty: Past, present, and future, *Environ. Sci. Technol.*, 47(24), 14258–14266, doi:10.1021/es403446m, 2013.
- Rohrbacher, A. and Kuwayama, T.: Fire Influences on O₃ levels: Insights into California O₃ Sensitivity using Ground and Satellite Measurements, In preparation.
- Schroeder, J. R., Crawford, J. H., Fried, A., Walega, J., Weinheimer, A., Wisthaler, A., Müller, M., Mikoviny, T., 640 Chen, G., Shook, M., Blake, D. R. and Tonnesen, G. S.: New insights into the column CH₂O/NO₂ ratio as an indicator of near-surface ozone sensitivity, *J. Geophys. Res. Atmos.*, 122(16), 8885–8907, doi:10.1002/2017JD026781, 2017.
- Seinfeld, J. H. and Spyros N. Pandis.: *Atmospheric Chemistry and Physics*, Third Edit., John Wiley & Sons, Inc, Hoboken., 2016.



- Shah, R. U., Coggon, M. M., Gkatzelis, G. I., McDonald, B. C., Tasoglou, A., Huber, H., Gilman, J., Warneke, C.,
645 Robinson, A. L. and Presto, A. A.: Urban Oxidation Flow Reactor Measurements Reveal Significant Secondary
Organic Aerosol Contributions from Volatile Emissions of Emerging Importance, *Environ. Sci. Technol.*, 54(2), 714–
725, doi:10.1021/acs.est.9b06531, 2020.
- Sillman, S.: The use of NO_y , H_2O_2 , and HNO_3 as indicators for ozone- NO_x -hydrocarbon sensitivity in urban
locations, *J. Geophys. Res.*, 100(D7), 14175, doi:10.1029/94JD02953, 1995.
- 650 Sillman, S.: The relation between ozone, $\text{NO}(x)$ and hydrocarbons in urban and polluted rural environments, *Atmos.*
Environ., 33(12), 1821–1845, doi:10.1016/S1352-2310(98)00345-8, 1999.
- Simon, H., Reff, A., Wells, B., Xing, J. and Frank, N.: Ozone trends across the United States over a period of
decreasing NO_x and VOC emissions, *Environ. Sci. Technol.*, 49(1), 186–195, doi:10.1021/es504514z, 2015.
- De Smedt, I., Theys, N., Yu, H., Danckaert, T., Lerot, C., Compennolle, S., Van Roozendael, M., Richter, A., Hilboll,
655 A., Peters, E., Pedergnana, M., Loyola, D., Beirle, S., Wagner, T., Eskes, H., Van Geffen, J., Folkert Boersma, K. and
Veeffkind, P.: Algorithm theoretical baseline for formaldehyde retrievals from S5P TROPOMI and from the QA4ECV
project, *Atmos. Meas. Tech.*, 11(4), 2395–2426, doi:10.5194/amt-11-2395-2018, 2018.
- South Coast AQMD: Facility-Based Mobile Source Measure focused on reducing emissions associated with vehicles
and mobile equipment operating in and out of warehouse distribution centers. [online] Available from:
660 [https://www.aqmd.gov/home/air-quality/clean-air-plans/air-quality-mgt-plan/facility-based-mobile-source-](https://www.aqmd.gov/home/air-quality/clean-air-plans/air-quality-mgt-plan/facility-based-mobile-source-measures/warehs-distr-wkng-grp)
[measures/warehs-distr-wkng-grp](https://www.aqmd.gov/home/air-quality/clean-air-plans/air-quality-mgt-plan/facility-based-mobile-source-measures/warehs-distr-wkng-grp) (Accessed 12 May 2021), 2021.
- Steiner, A. L., Tonse, S., Cohen, R. C., Goldstein, A. H. and Harley, R. A.: Influence of future climate and emissions
on regional air quality in California, *J. Geophys. Res.*, 111(D18), D18303, doi:10.1029/2005JD006935, 2006.
- Steiner, A. L., Cohen, R. C., Harley, R. A., Tonse, S., Millet, D. B., Schade, G. W. and Goldstein, A. H.: VOC
665 reactivity in central California: Comparing an air quality model to ground-based measurements, *Atmos. Chem. Phys.*,
8(2), 351–368, doi:10.5194/acp-8-351-2008, 2008.
- Tonnesen, G. S. and Dennis, R. L.: Analysis of radical propagation efficiency to assess ozone sensitivity to
hydrocarbons and NO_x 1. Local indicators of instantaneous odd oxygen production sensitivity, *J. Geophys. Res.*
Atmos., 105(D7), 9213–9225, doi:10.1029/1999JD900371, 2000.
- 670 U.S. Global Change Research Program: Climate science special report: Fourth national climate assessment, volume
I, edited by D. J. Wuebbles, D. W. Fahey, K. A. Hibbard, D. J. Dokken, B. C. Stewart, and T. K. Maycock., 2018.
- US EPA: 2017 National Emissions Inventory Technical Support Documentation, , (April), 486 [online] Available
from: <https://www.epa.gov/air-emissions-inventories/2017-national-emissions-inventory-nei-data> (Accessed 16 April
2021a), 2020.
- 675 US EPA: Integrated Science Assessment (ISA) for ozone and related photochemical oxidants (Final Report), U.S.
Environ. Prot. Agency, Washington, DC, EPA/600/R-20/012, 2020 [online] Available from:
<https://www.epa.gov/isa/integrated-science-assessment-isa-ozone-and-related-photochemical-oxidants> (Accessed 9
June 2021b), 2020.
- US EPA: Criteria Air Pollutants | US EPA, US EPA [online] Available from: [https://www.epa.gov/criteria-air-](https://www.epa.gov/criteria-air-pollutants)
680 [pollutants](https://www.epa.gov/criteria-air-pollutants) (Accessed 1 April 2021), 2021.



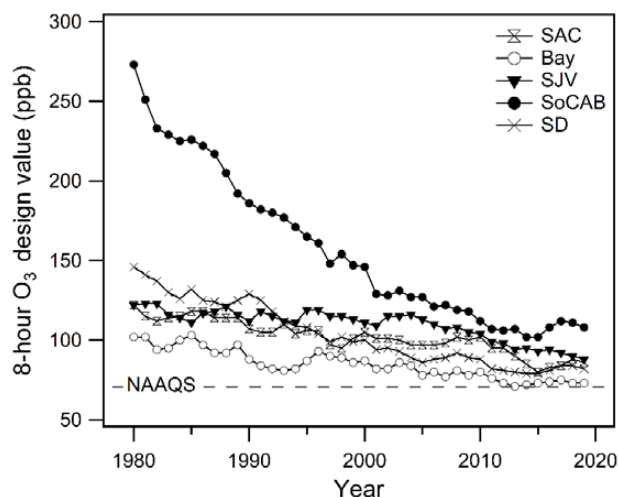
685 Veefkind, J. P., Aben, I., McMullan, K., Förster, H., de Vries, J., Otter, G., Claas, J., Eskes, H. J., de Haan, J. F.,
Kleipool, Q., van Weele, M., Hasekamp, O., Hoogeveen, R., Landgraf, J., Snel, R., Tol, P., Ingmann, P., Voors, R.,
Kruizinga, B., Vink, R., Visser, H. and Levelt, P. F.: TROPOMI on the ESA Sentinel-5 Precursor: A GMES mission
for global observations of the atmospheric composition for climate, air quality and ozone layer applications, *Remote*
Sens. Environ., 120(2012), 70–83, doi:10.1016/j.rse.2011.09.027, 2012.

Vigouroux, C., Langerock, B., Augusto, C., Aquino, B., Blumenstock, T. and Cheng, Z.: TROPOMI – Sentinel-5
Precursor formaldehyde validation using an extensive network of ground-based Fourier-transform infrared stations, ,
3751–3767, 2020.

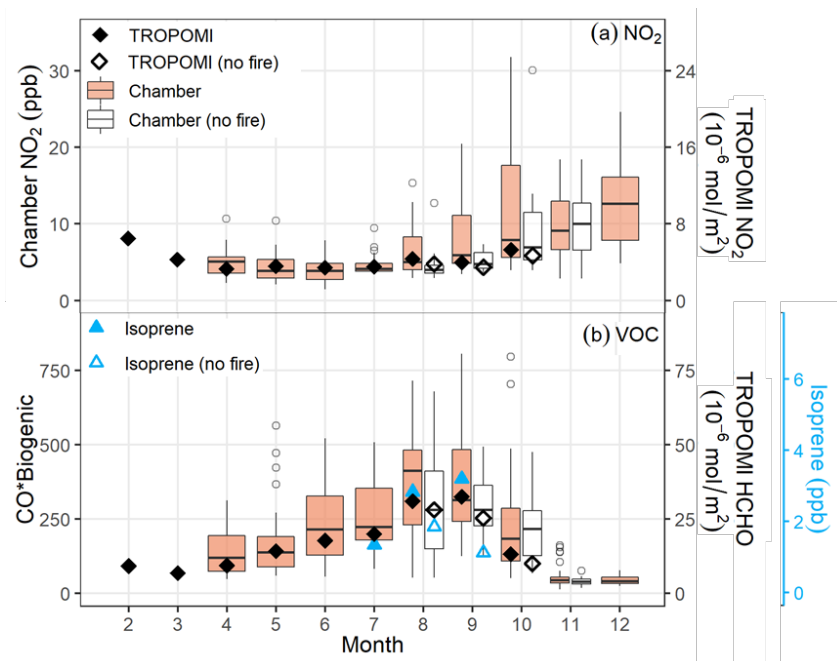
690 Weaver, C. P., Liang, X. Z., Zhu, J., Adams, P. J., Amar, P., Avise, J., Caughey, M., Chen, J., Cohen, R. C., Cooter,
E., Dawson, J. P., Gilliam, R., Gilliland, A., Goldstein, A. H., Grambsch, A., Grano, D., Guenther, A., Gustafson, W.
I., Harley, R. A., He, S., Hemming, B., Hogrefe, C., Huang, H. C., Hunt, S. W., Jacob, D. J., Kinney, P. L., Kunkel,
K., Lamarque, J. F., Lamb, B., Larkin, N. K., Leung, L. R., Liao, K. J., Lin, J. T., Lynn, B. H., Manomaiphiboon, K.,
Mass, C., Mckenzie, D., Mickley, L. J., O’Neill, S. M., Nolte, C., Pandis, S. N., Racherla, P. N., Rosenzweig, C.,
Russell, A. G., Salathé, E., Steiner, A. L., Tagaris, E., Tao, Z., Tonse, S., Wiedinmyer, C., Williams, A., Winner, D.
695 A., Woo, J. H., Wu, S. and Wuebbles, D. J.: A preliminary synthesis of modeled climate change impacts on U.S.
regional ozone concentrations, *Bull. Am. Meteorol. Soc.*, 90(12), 1843–1863, doi:10.1175/2009BAMS2568.1, 2009.

William, D. R. and Burke, A.: Final 2016 Air Quality Management Plan., 2016.

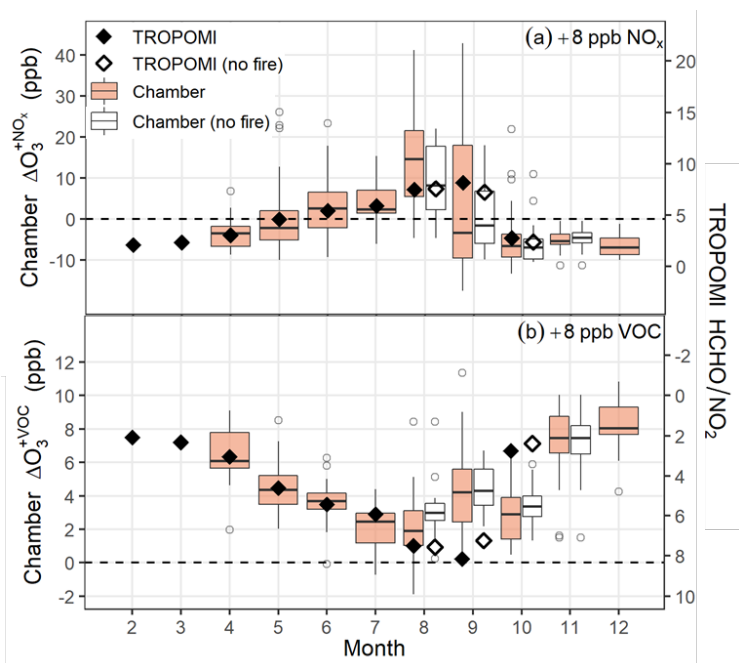
Zhang, Q., Zhou, S., Collier, S., Jaffe, D., Onasch, T., Shilling, J., Kleinman, L. and Sedlacek, A.: Understanding
composition, formation, and aging of organic aerosols in wildfire emissions via combined mountain top and airborne
700 measurements, *ACS Symp. Ser.*, 1299, 363–385, doi:10.1021/bk-2018-1299.ch018, 2018.



705 **Figure 1.** 8-hour O₃ design value in 5 air basins in California from 1980 to 2019. Dash line is the 2015 8-hr O₃ NAAQS (= 70 ppb). 5 air basins include Sacramento Valley (SAC), San Francisco Bay area (Bay), San Joaquin Valley (SJV), South Coast Air Basin (SoCAB), San Diego County (SD). Data collected from California Air Resources Board (<https://www.arb.ca.gov/adam>).

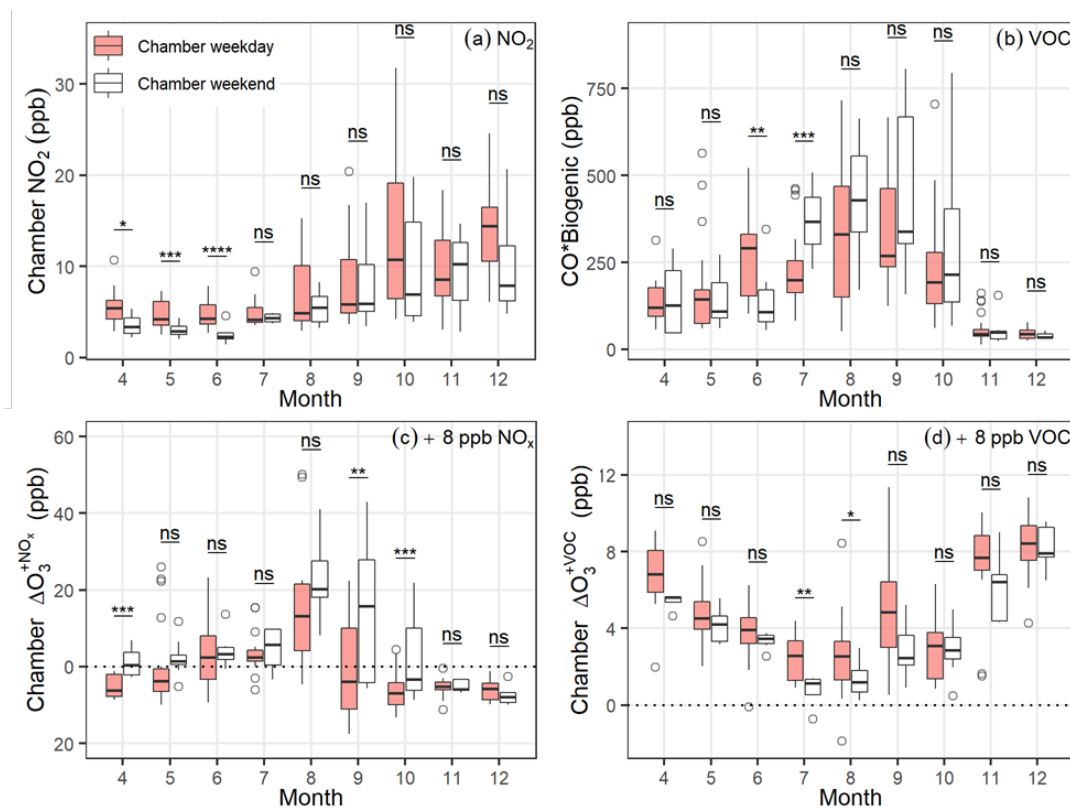


710 Figure 2. Monthly concentrations of NO_2 (panels a) and $\text{CO}^*\text{Biogenic}/\text{HCHO}/\text{Isoprene}$ (panels b) from February to December 2020. Ground-based chamber measurements use the left axis with results shown as box and whisker plots. TROPOMI measurements use the right axis and are shown as diamonds. Isoprene from ground monitoring station shown as blue triangles. The open box and points show the results after removing wildfire days.



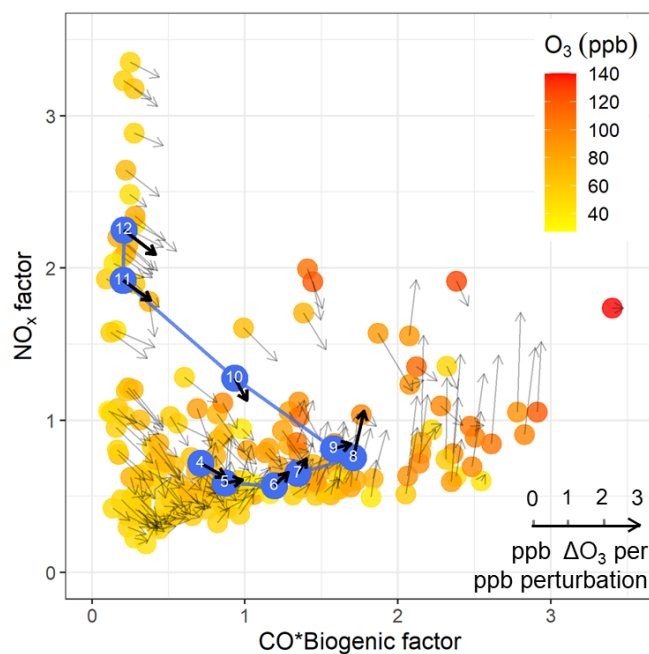
715

Figure 3. Monthly variance of TROPOMI HCHO/NO₂ (diamond) and ΔO₃ (box) due to NO_x addition (ΔO₃^{+NO_x}) and VOC addition (ΔO₃^{+VOC}) from April to December including wildfire days (top) and without wildfire days (bottom).



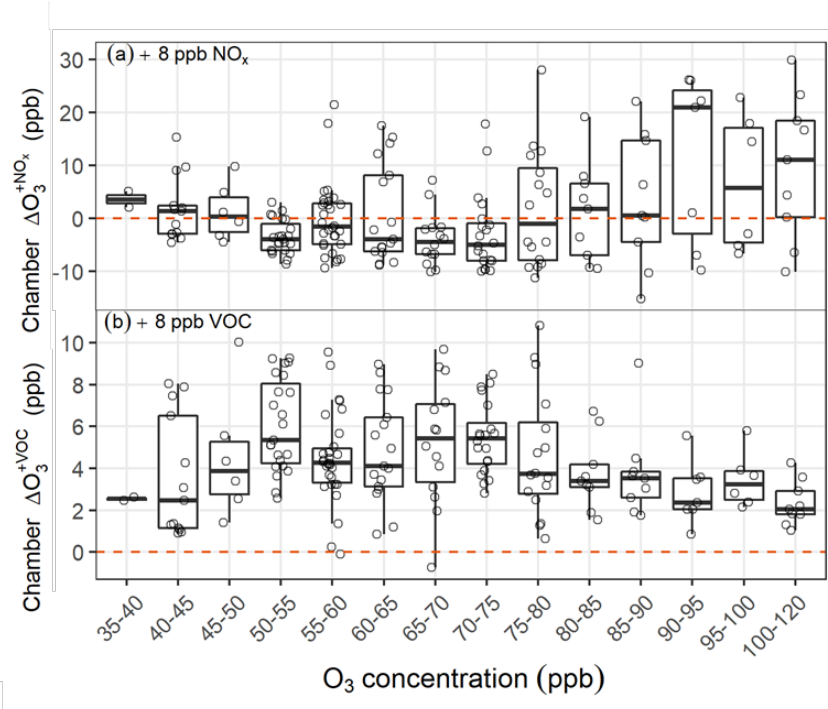
720

Figure 4. Weekday (solid box) and weekend (open box) monthly-average concentrations of NO_2 and $\text{CO}^*\text{biogenic}$ (panels a, b), and $\Delta\text{O}_3^{+\text{NO}_x}$ and $\Delta\text{O}_3^{+\text{VOC}}$ (panels c, d) from April to December, 2020 after removing wildfire days. The stars above each box and whisker plot represent the significance of the weekday vs weekend difference. (*: p value < 0.1, **: p value < 0.05, ***: p value < 0.01, ****: p value < 0.001, ns (not significant): p value \geq 0.1)



725

Figure 5. Measured O₃ isopleth diagram. The NO_x and CO*Biogenic factor is calculated by the daily value divided by averaged value. The O₃ concentration is the daily O₃ concentration in the basecase chamber after 3 hours UV exposure. Arrows represent the O₃ sensitivity. The blue dots are the monthly averaged values, the blue line shows the seasonal cycle in the O₃ isopleth diagram. Days influenced by wildfires are removed from the plot.



730 Figure 6. Boxplot of O₃ sensitivity to NO_x and VOC at a certain bin of O₃ concentration after 3-hour UV exposure in basecase chamber (#2).

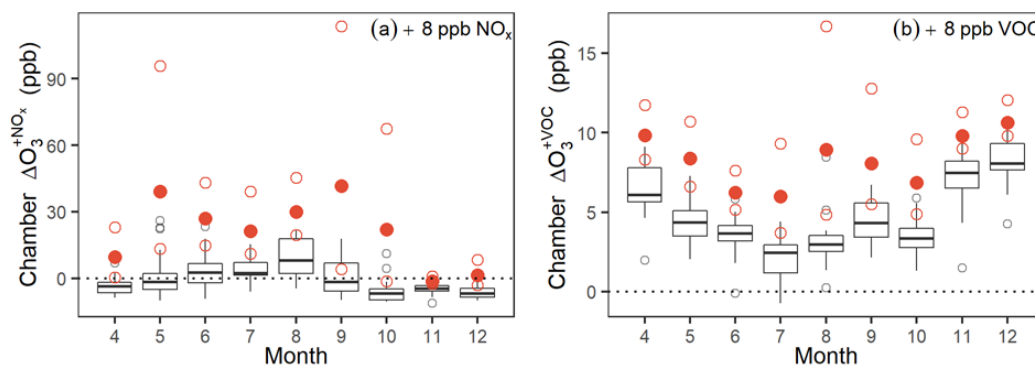
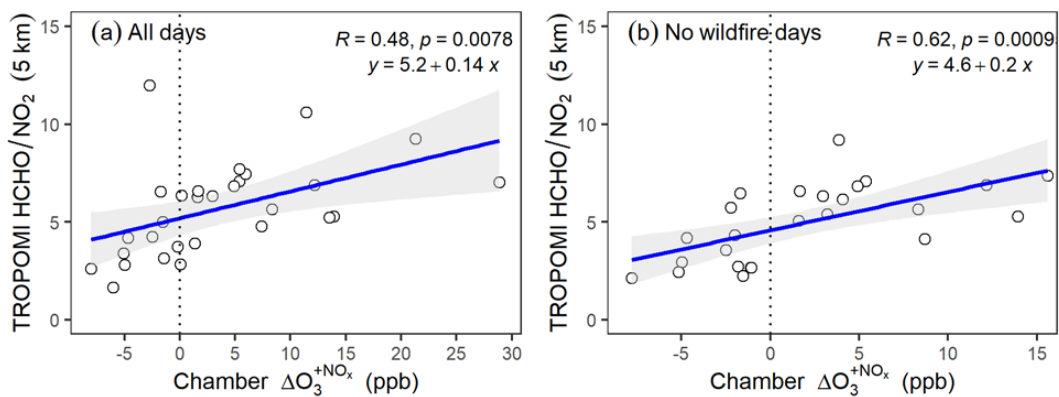
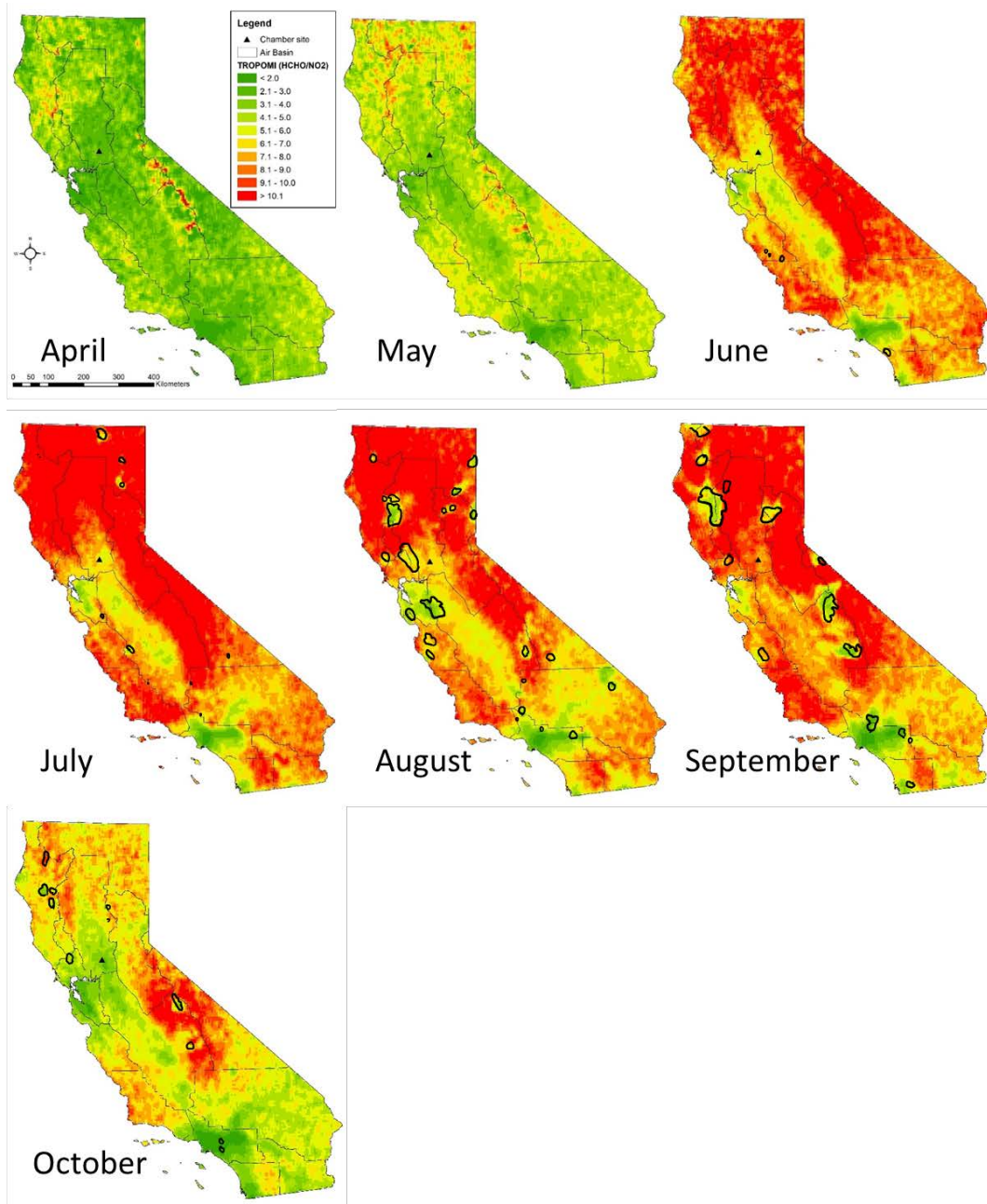


Figure 7. 3-year return level (red dot) and 95% confidence interval (red open dot) from extreme value analysis of O₃ sensitivity to NO_x and VOC.



735

Figure 8. Correlation between weekly averaged TROPOMI HCHO/NO₂ at 5 km circular buffers and the weekly averaged $\Delta O_3^{+NO_x}$ from ground-based measurement.



740

Figure 9. Spatial distribution of TROPOMI satellite (HCHO/NO_2) ratios in California for April – October 2020. The black bold line circles the burned area in each month detected by MODIS from Fire Information for Resource Management System (FIRMS). The NO_x -limited conditions correspond to HCHO/NO_2 ratios above 4.6.

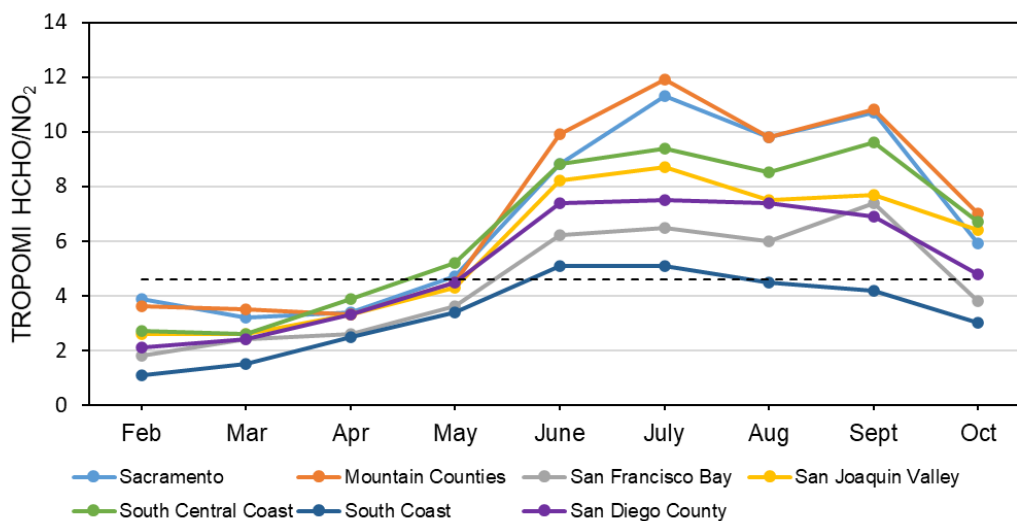


Figure 10. Monthly variations of TROPOMI HCHO/NO₂ for 7 major O₃-nonattainment air basins in California. Dashed line is the threshold of O₃ sensitivity regime (HCHO/NO₂ = 4.6).